Biogeosciences, 7, 3851–3867, 2010
www.biogeosciences.net/7/3851/2010/
doi:10.5194/bg-7-3851-2010

Biogeosciences

Air-Sea CO_2 fluxes on the Scotian Shelf: seasonal to multi-annual variability

E. H. Shadwick[1], H. Thomas[1], A. Comeau[1], S. E. Craig[1], C. W. Hunt[2], and J. E. Salisbury[2]

[1]Department of Oceanography, Dalhousie University, Halifax, NS, Canada
[2]Ocean Processes Analysis Laboratory, University of New Hampshire, Durham, NH, USA

Received: 24 June 2010 – Published in Biogeosciences Discuss.: 8 July 2010
Revised: 12 November 2010 – Accepted: 15 November 2010 – Published: 26 November 2010

Abstract. We develop an algorithm to compute pCO_2 in the Scotian Shelf region (NW Atlantic) from satellite-based estimates of chlorophyll-*a* concentration, sea-surface temperature, and observed wind speed. This algorithm is based on a high-resolution time-series of pCO_2 observations from an autonomous mooring. At the mooring location (44.3° N and 63.3° W), the surface waters act as a source of CO_2 to the atmosphere over the annual scale, with an outgassing of $-1.1\,\mathrm{mol\,C\,m^{-2}\,yr^{-1}}$ in 2007/2008. A hindcast of air-sea CO_2 fluxes from 1999 to 2008 reveals significant variability both spatially and from year to year. Over the decade, the shelf-wide annual air-sea fluxes range from an outgassing of $-1.70\,\mathrm{mol\,C\,m^{-2}\,yr^{-1}}$ in 2002, to -0.02 $\mathrm{mol\,C\,m^{-2}\,yr^{-1}}$ in 2006. There is a gradient in the air-sea CO_2 flux between the northeastern Cabot Strait region which acts as a net sink of CO_2 with an annual uptake of 0.50 to $1.00\,\mathrm{mol\,C\,m^{-2}\,yr^{-1}}$, and the southwestern Gulf of Maine region which acts as a source ranging from -0.80 to $-2.50\,\mathrm{mol\,C\,m^{-2}\,yr^{-1}}$. There is a decline, or a negative trend, in the air-sea pCO_2 gradient of 23 µatm over the decade, which can be explained by a cooling of 1.3 °C over the same period. Regional conditions govern spatial, seasonal, and interannual variability on the Scotian Shelf, while multi-annual trends appear to be influenced by larger scale processes.

1 Introduction

The rise in atmospheric carbon dioxide (CO_2) from anthropogenic emissions is partially offset by the oceans' CO_2 uptake (Sabine et al., 2004); direct estimates of this uptake require accurate measurements of the partial pressure of CO_2 (pCO_2) in the surface-ocean, and knowledge of its seasonal and interannual variability. Measurements of pCO_2 in the open ocean have increased considerably (Boutin and Merlivat, 2009; Takahashi et al., 2009; Watson et al., 2009). The increased acquisition of pCO_2 data has facilitated a deeper understanding of the variability of CO_2 fluxes, particularly for the North Atlantic Ocean (Schuster and Watson, 2007; Thomas et al., 2008; Schuster et al., 2009; Metzl et al., 2010). These investigations have been complemented by the application of satellite data (Lefèvre et al., 2002; Olsen et al., 2008; Chierici et al., 2009) and modelling studies to respectively increase both spatial and temporal coverage, and to gain a mechanistic understanding of the systems (Etcheto et al., 1999; Wanninkhof et al., 2007; Lefévre et al., 2008; Padin et al., 2008; Thomas et al., 2008; Ullman et al., 2009). However, while fundamental understanding of air-sea CO_2 exchange in coastal oceans has yet to be achieved, the few available studies provide evidence for highly variable CO_2 fluxes in these regions (Cai et al., 2006; Thomas et al., 2007; Borges et al., 2008). Despite relatively large CO_2 fluxes in coastal oceans (Tsunogai et al., 1999; Thomas et al., 2004), the temporal and spatial variability of pCO_2 remains particularly poorly understood (Borges, 2005; Borges et al., 2005; Cai et al., 2006; Laruelle et al., 2010), and the reliability of assessments employing space-borne sensors in these regions has not been established (Lohrenz and Cai, 2006; Salisbury et al., 2008).

In the present study we combine highly temporally resolved autonomous observations, in-situ data from monthly shipboard sampling, and space-borne observations to investigate the variability of CO_2 fluxes in the Scotian Shelf region of the Canadian northwestern Atlantic. The use of these three independent observational techniques allows an assessment of the governing processes at seasonal, interannual, and multi-annual time scales to be made.

Correspondence to: E. H. Shadwick
(elizabeth.shadwick@dal.ca)

Published by Copernicus Publications on behalf of the European Geosciences Union.

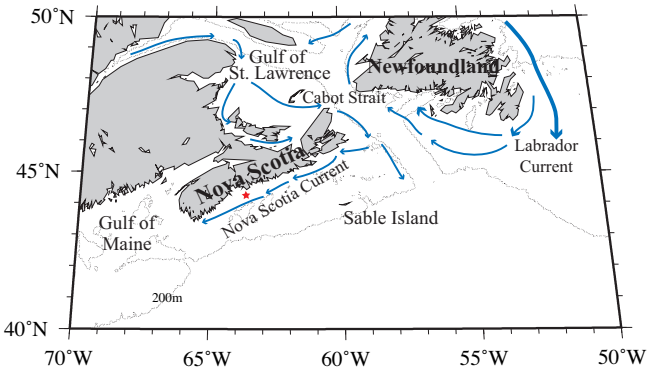

Fig. 1. The hydrographic setting on the Scotian Shelf (see, for example, Loder et al., 1997; Hannah et al., 2001). The position of the CARIOCA buoy (red star) and the Sable Island Meteorological Station are indicated.

2 Oceanographic setting

The Scotian Shelf comprises a 700 km long section of the continental shelf off the Canadian province of Nova Scotia. The Scotian Shelf is bounded by the Gulf of St. Lawrence and Cabot Strait to the north and by the Gulf of Maine to the southwest, varying in width from 120 to 240 km (Fig. 1). The Scotian Shelf is uniquely located at the junction of the North Atlantic sub-polar and sub-tropical gyres, downstream of the St. Lawrence River system (Loder et al., 1997; Hannah et al., 2001). The seasonal shelf-scale circulation is dominated by the Nova Scotia Current flowing to the southwest roughly parallel to the coast, and an extension of the Labrador Current, flowing in the same direction, along the shelf edge (Loder et al., 1997). The water masses on the northeastern North American coast are well-studied (Bigelow, 1927; Hachey, 1942; Chapman and Beardsley, 1989; Loder et al., 1998). As many as eight distinct water masses have been identified in the Scotian Shelf region (Khatiwala et al., 1999; Houghton and Fairbanks, 2001). However, for simplicity, the water column on the Scotian Shelf can be characterized by a two-layer system in winter when relatively fresh shelf water overlies more saline slope water. In summer, it is characterized by a three-layer system with the development of a warm, shallow, surface layer overlying the two-layer system (Loder et al., 1997).

The seasonal cycle of sea-surface temperature on the Scotian Shelf has an annual range of roughly 16 °C to 20 °C, which is among the largest in the world (Umoh and Thompson, 1994). The southwestern outflow from Cabot Strait is the major source of freshwater to the region. Salinity on the Scotian Shelf increases with distance offshore due to the northward transport of Gulf Stream waters. In autumn, the warmest surface temperature is observed in the central Scotian Shelf, increasing with the distance from shore. The peak in river discharge from the St. Lawrence is delivered to the Scotian Shelf between June and October; surface salinity is typically decreased by 1 unit, from roughly 30.5 to 29.5, as a result of this input (Loder et al., 1997).

Coastal upwelling events on the Scotian Shelf have long been recognized (Hachey, 1935; Petrie, 1983). Upwelling events have frequently been observed in the near-shore regions of the Scotian Shelf, and modeling studies have reproduced these observed events (Petrie, 1983; Donohue, 2000). Furthermore, these events may play a role in initiating and sustaining the spring phytoplankton bloom by displacing nutrient-depleted surface water and bringing nutrient-rich waters to the surface (Greenan et al., 2004). Convection occurs in the winter season on the Scotian Shelf. In this region wind speed exerts some control over the depth of convective mixing; an increase in wind strength removes more heat from the surface waters and deepens the extent of convection.

3 Methods

Hourly, autonomous observations of surface water pCO_2 (µatm), chlorophyll-*a* fluorescence (F_{Chl}), and sea-surface temperature (SST), were made using a CARIOCA buoy moored roughly 30 km offshore from Halifax, at 44.3° N and 63.3° W, between April 2007 and June 2008. Hourly CARIOCA data were uploaded and transmitted daily via the ARGOS satellite system. The pCO_2 measurements were made by an automated spectrophotometric technique (Bates et al., 2000; Bakker et al., 2001; Copin-Montégut et al., 2004). A Sea-Bird (SBE 41) conductivity and temperature sensor was used to measure temperature (°C) and to determine salinity; chlorophyll-*a* fluorescence (µg l^{-1}) was determined by a WET Labs miniature fluorometer (WETstar).

Non-photochemical effects that are related to the intensity of the incoming solar radiation may decrease F_{Chl} up to 80% during the day (Kiefer, 1973). This effect can be avoided by using night-time data which, to a large extent, are free of the effects of non-photochemical quenching, for fluorometer calibration. Night-time data were taken as a mean F_{Chl} between 03:00 and 06:00 UTC (or 11:00 and 02:00 LT); data points were temporally interpolated to match discrete chlorophyll-*a* measurements (Chl-*a* [mg m^{-3}]) from monthly or twice-monthly occupations at the mooring site. chlorophyll-*a* concentration was determined fluorometrically in a Turner Designs fluorometer using the acid ratio technique (Strickland and Parsons, 1972) for seawater samples collected at 3, 5, or 10 m depth. A linear regression ($r^2 = 0.76$, N=29, $p < 0.001$) was used to determine the relationship between the F_{Chl} and Chl-*a*, and applied to the CARIOCA fluorescence-derived chlorophyll-*a* time-series (Chl_F [mg m^{-3}], see Table 1 for a summary of notation used to distinguish between the time-series of chlorophyll-*a*).

Wind speed (m s^{-1}) and atmospheric CO_2 (µatm) were measured hourly by Environment Canada at the Sable Island Meteorological Station (43.9° N and 60.3° W) at a height of 10 m using a sonic anemometer and an open-path infra-red

Table 1. Notation for different time-series of chlorophyll-*a*, in units of mg m^{-3}.

Symbol	Description
F_{Chl}	chlorophyll-*a* fluorescence determined by CARIOCA fluorometer
Chl-*a*	discrete chlorophyll-*a* from the mooring station determined using the acid ratio technique
Chl_F	fluorescence-derived chlorophyll-*a* time series used in Eq. 2
$\mathrm{Chl}_{\mathrm{SAT}}$	satellite derived chlorophyll-*a* concentration

CO_2 analyzer (Fig. 1). Monthly mean values of surface water pCO_2, Chl_F, and SST, were computed from the CARIOCA time series, comprising more than 2000 observations over a 14-month period. Monthly integrals of the gas transfer velocity (k [cm hr^{-1}]) were computed from hourly winds and the formulation of Wanninkhof (1992). It has been suggested that the parameterization of Wanninkhof (1992) may overestimate the gas transfer velocity (Sweeney et al., 2007). The uncertainty associated with the monthly air-sea flux (20%) was estimated from the difference between the flux computed with the parameterization of Wanninkhof (1992) and the flux computed with the parameterization of Nightingale et al. (2000); the accuracy of the flux computations is relatively low due to the large error associated with the gas transfer parameterization (Naegler et al., 2006; Sweeney et al., 2007; Watson et al., 2009). The air-sea CO_2 fluxes (F [mol C m^{-2} month^{-1}]) were computed via:

$$F = k\alpha\Delta pCO_2, \tag{1}$$

where α is the coefficient of solubility (Weiss, 1974) and ΔpCO_2 is the gradient in pCO_2 between the ocean and the atmosphere ($\Delta pCO_2 = pCO_2^{\mathrm{Ocean}} - pCO_2^{\mathrm{Atm}}$). It has been shown that the winds at Sable Island are representative of the winds over the Scotian Shelf (Petrie and Smith, 1977); values of k computed from Sable Island winds were therefore used in the flux computations in each grid box. Hourly winds ranged from 0 m s^{-1} to roughly 30 m s^{-1}. Please note that this may cause an overestimate of wind speed, and subsequently the gas transfer velocity, in the near-shore regions, and an underestimate of wind speed for regions further offshore than the Sable Island Station. A negative flux indicates a transfer from the ocean into the atmosphere.

4 Results

4.1 Multiple Linear Regression

A multiple linear regression (MLR) (Eq. 1) was applied using monthly mean values of pCO_2, Chl_F, SST, and the gas transfer velocity, k, as predictor variables (i.e. N=14). The regression was also applied to the hourly (night-time) observations ($n = 2000$), and the resulting regression coefficients were similar to those presented in Eq. (2). The choice of monthly means to generate Eq. (2) was made for temporal consistency with the remotely-sensed data obtained on a monthly timescale which was used, along with Eq. 2 to compute pCO_2, and is described in Sect. 4.2. The April value of Chl_F acted as a leverage point, dominating the regression, and allowing the pCO_2 minimum to be reproduced by the model. During the remainder of the year, pCO_2 is influenced to a lesser degree by Chl_F, and more strongly by the annual cycle of SST.

$$pCO_2 = 354.4 - 24.6\ \mathrm{Chl}_F + 4.6\ \mathrm{SST} + 3.7k \tag{2}$$

$$\mathrm{X_t} = \frac{1.7}{12}\Delta t \tag{3}$$

Surface water pCO_2 on the Scotian Shelf was reconstructed from January 1999 to December 2008 using Eq. (2). A correction term, $\mathrm{X_t}$ (µatm) (Eq. 3), was applied to account for the rise of surface ocean pCO_2 of approximately 1.7 µatm yr^{-1}, relative to January 1999, due to the uptake of anthropogenic atmospheric CO_2 (Thomas et al., 2008). This term is added to the right hand side of Eq. (2) for each month "t", with Δt (months) equal to the number of months since January 1999. For example, in February 1999 $\mathrm{X_t}$ would be computed with: $\mathrm{X_t}$=(1.7/12) µatm. The multiple linear regression (Eq. 2) is applied to absolute values of Chl_F, SST, and k, to compute monthly, values of pCO_2. This approach allows the use of predictor variables that can be observed remotely, and captures the underlying physical and biological mechanisms in the system.

Further information regarding the predictive capacity of Chl_F, SST, and k to estimate pCO_2 was gained by computing the normalized, or β coefficients. These coefficients are dimensionless and directly comparable allowing an assessment of the relative contribution, or weight, of each of the predictor variables (i.e. Chl_F, SST, and k) in the estimate of pCO_2 (Table 2). Chl_F makes the strongest contribution, and both the Chl_F and SST coefficients are roughly double the magnitude of the k coefficient (Table 2). The standard error associated with the computation of pCO_2 using the MLR is 13 µatm, and the associated $r^2 = 0.81$. The inclusion of the gas transfer velocity (k) in the MLR reduced the standard error (from 19 µatm) and increased the r^2 (from 0.73). The gas transfer velocity was used to reflect wind stress, as opposed to wind speed, the former being the quantity of interest when computing air-sea CO_2 fluxes.

Table 2. Non-standardized, or "B" regression coefficients (see Eq. 2) and the normalized, β coefficients.

	Chl_F	SST	k
B	−24.6	4.6	3.7
β	−0.65	0.50	0.25

4.2 Interpretation of regression coefficients

The value of the Chl_F regression coefficient obtained in Eq. (2) ($-24.6\,\mu atm\ (mg\ m^{-3})^{-1}$), is dominated by the spring bloom, and is consistent with a value obtained in a recent regression study in the North Atlantic south of Greenland (Chierici et al., 2009). The Chl_F coefficient corresponds to a ratio of inferred net inorganic carbon assimilation to accumulated chlorophyll on the order of 115 mg C (mg Chl-a)$^{-1}$. This estimate was made using a Revelle Factor of 13; for every mg m^{-3} of Chl-a there is a change in pCO_2 of -24.6 µatm (Eq. 2). Using an annual mean pCO_2 of 420 µatm, and an annual mean value of dissolved inorganic carbon (DIC) of 1950 µmol kg^{-1} (Shadwick et al., 2011a), the ratio of DIC to Chl-a, or C:Chl, is roughly 115 mg C (mg Chl-a)$^{-1}$. This estimate is somewhat higher than literature values of ∼50 mg C (mg Chl-a)$^{-1}$) (Platt et al., 1991). This difference may be explained by the fact that the literature C:Chl ratios do not account for losses of chlorophyll both due to sinking - whereby chlorophyll leaves the system but the inorganic carbon deficit remains- and grazing leading to the accumulation of detritus and heterotrophic biomass (Weeks et al., 1993; Banse, 1995; Taylor et al., 1997).

The SST regression coefficient obtained in Eq. 2 (4.6 µatm (°C)$^{-1}$) is lower than the thermodynamically expected value, which would be roughly 16 µatm (°C)$^{-1}$ at 400 µatm (Takahashi et al., 2002). The SST regression coefficient obtained is composed of the competing influences of the thermodynamic temperature dependence of pCO_2, and the pCO_2 dependence on biological processes at the monthly time scale. The spring and summer pCO_2 drawn-down occurs in the period of nutrient depletion, but is not necessarily resolved by the chlorophyll record (Shadwick et al., 2011). Furthermore, the SST coefficient likely comprises additional effects of changes in salinity, which are also anti-correlated with temperature. However, these salinity changes play only a minor role in changing pCO_2 due to the opposing effects of alkalinity and dissolved inorganic carbon on pCO_2 (Shadwick et al., 2011a) (see Appendix for more detailed discussion of the SST coefficient).

The gas transfer velocity (k) here serves as a directly assessable representation of the mixed-layer depth. Mixed-layer depth was determined from observed monthly temperature profiles using the Levitus (1982) temperature criterion, which defines the mixed-layer as the depth at which the change from the surface temperature is 0.5 °C. Mixed-layer depth, is plotted versus monthly values of gas transfer velocity for the year 2008 in Fig. 2. A linear regression revealed a significant correlation between the two variables ($r^2 = 0.79$, N=12, $p < 0.001$). By using k, stronger winds, and a deeper mixed-layer, make a large contribution to the monthly value of pCO_2, while weaker winds, and a shallow mixed-layer, make a smaller, though still positive contribution to pCO_2. Mechanistically, with increasing winds, k represents the deepening of the mixed-layer in autumn and winter, which implies an intrusion of CO_2-rich subsurface water into the surface-layer. On the other hand, in spring and particularly in summer, weak winds, and thus lower values of k, yield lower values of pCO_2. In summer, if the moderate biological activity is confined to a shallower mixed-layer, it has a stronger impact on the pCO_2 (or the CO_2 concentration), than if it occurred within a deeper mixed-layer. In the regression model presented here, the k coefficient thus helps assign a third dimension to the two-dimensional satellite view. This is required to parameterize the CO_2 concentration changes as driver of the air-sea CO_2 flux rather than changes in the CO_2 inventory. The effect of gas exchange itself plays a subordinate role in altering water column CO_2 concentrations on the short, monthly, time scales applicable here.

The change in pCO_2 due to each of the predictor variables was computed using Eq. (4–6), using the 12 monthly mean values of Chl_F, SST and k (Fig. 3). For example, the change in pCO_2 due to chlorophyll, $pCO_2(Chl_F)$, was computed (Eq. 4) by keeping SST and k constant, at their initial, January 2008, values (subscript "J"), and allowing Chl_F to vary. The change in pCO_2 due to SST and k were similarly computed.

$$pCO_2(Chl_F) = 354.4 - 24.6\ Chl_F + 4.6\ SST_J + 3.7k_J \quad (4)$$

$$pCO_2(SST) = 354.4 - 24.6\ Chl_{FJ} + 4.6\ SST + 3.7k_J \quad (5)$$

$$pCO_2(k) = 354.4 - 24.6\ Chl_{FJ} + 4.6\ SST_J + 3.7k \quad (6)$$

The influence of Chl_F (Fig. 3 in green) dominates the total change (in black) in April, and plays a lesser, though non-zero, role during the rest of the year, reflecting the contribution of the late summer production (Shadwick et al., 2011a). The SST control (Fig. 3 in red) increases pCO_2 from April to September, decreases pCO_2 from September to December, and is near neutral from December to April. The gas transfer velocity (Fig. 3 in blue) acts to increases pCO_2 most strongly in the autumn and winter when wind driven and convective mixing enhances the entrainment of high-carbon water into the surface layer.

4.3 Spatial extrapolation and validation

Seven 2°×2° grid boxes, covering the Scotian Shelf were defined (Fig. 4). The MLR (Eq. 2) was used to generate a hindcast of pCO_2 that was extrapolated spatially using monthly means of satellite-derived chlorophyll-a concentration (Chl_{SAT} [mg m^{-3}]) and SST, along with the gas transfer

Table 3. Comparison of pCO_2(MLR) with pCO_2(underway), pCO_2(DIC,TA), and pCO_2(CARINA) All values are in µatm. See also Figs. 6 and 7, and Fig. 4 for the locations of the grid boxes.

Date (mm/yyyy)	Box	pCO_2(MLR)	pCO_2(Underway)	pCO_2(DIC,TA)	pCO_2(CARINA)
05/2004	7	363			333
07/2004	7	417			393
06/2006	1	403			372
06/2006	3	415			363
06/2006	5	401			368
06/2006	7	406			367
09/2006	1	423		422	
09/2006	3	439		419	
09/2006	5	420		415	
10/2006	7	429		417	
02/2007	2	392		417	352
03/2007	2	354			264
04/2007	1	323	289	295	
04/2007	2	356	285		
04/2007	3	345	328	332	274
04/2007	4	349	305		
04/2007	5	307	298		301
04/2007	7	349	314	323	
07/2007	1	407			415
07/2007	2	392			387
07/2007	3	420			415
07/2007	5	409		332	401
07/2007	5	410		332	394
08/2007	1	414	420	426	
08/2007	2	433	430		
08/2007	4	439	430		
09/2007	1	421			406
10/2007	1	417	436	440	
10/2007	2	434	445		
10/2007	3	434	427	436	
10/2007	4	438	427		
10/2007	5	413	405	412	
10/2007	7	422	420	426	
04/2008	1	327	308	313	
04/2008	2	346	295		
04/2008	3	327	305	303	
04/2008	4	341	304	3	
04/2008	5	319	302	309	
04/2008	7	371	320	324	

velocity (*k)* computed with hourly winds measured at Sable Island (Fig. 5). The estimates of Chl_{SAT} were acquired from the Level 3 equal-area 9-km data from the Sea-viewing Wide Field-of-view Sensor (SeaWiFS) on the SeaStar platform, while SST was acquired from the Pathfinder AVHRR equal-area 9-km best-SST data product. The monthly Chl_{SAT} data were regressed against the (night-time calibrated), monthly mean, CARIOCA Chl_F time series, ($r^2 = 0.68$, N=14, $p < 0.002$) and scaled accordingly. This scaling was done primarily to account for low monthly mean values of Chl_{SAT} within grid box 1 (comprising the mooring location, Fig. 4) relative to the calibrated Chl_F time series, and it was assumed that the scaling was valid for all seven grid boxes. The relationship between Chl_F and Chl_{SAT} was roughly 1:1; the satellite derived mean chlorophyll estimate (over the $2^\circ \times 2^\circ$ grid box) was in good agreement with the data from the CARIOCA fluorometer. However, the CARIOCA buoy was moored near the coast, and the discrete Chl-*a* measurements were made at this location. There are shortcomings associated with SeaWiFS data in coastal regions due to the potentially high concentrations of colored dissolved organic matter (CDOM) and suspended particulate matter in coastal waters (Lohrenz and Cai, 2006; Salisbury et al., 2008) which may bias the Chl_{SAT} concentrations. The standard deviation for

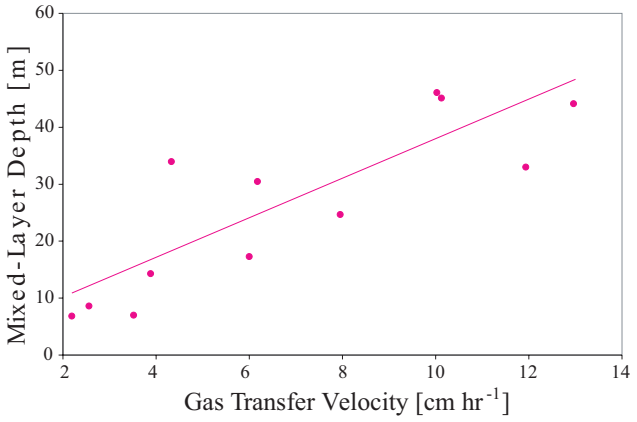

Fig. 2. The relationship between mixed-layer depth estimated from profiles of temperature at the mooring station, and gas transfer velocity computed from hourly winds measured at Sable Island (see Fig. 1).

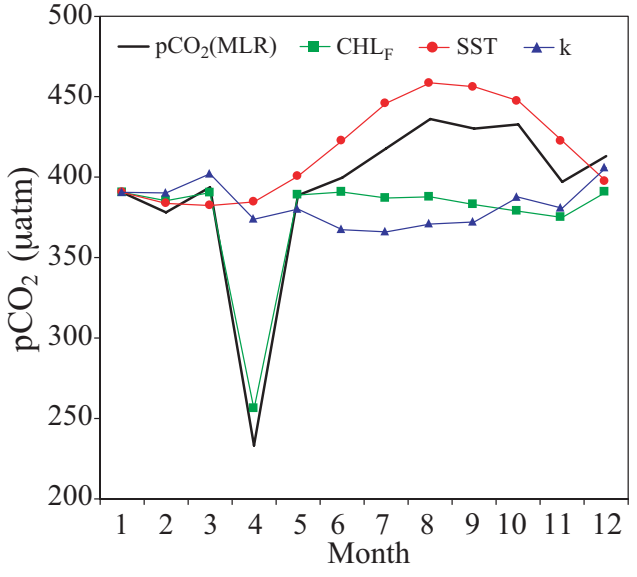

Fig. 3. The respective contributions from Chl_F (in green), SST (in red) and k (in blue) to pCO_2(MLR) (in black) at the mooring location (see Fig. 1) over the annual cycle.

the average monthly Chl_{SAT} concentration within a grid box (containing 576 pixels) ranged from 0.1 to 0.49 mg m^{-3}, with higher variation in the near-shore boxes.

The pCO_2(MLR) was validated against measurements of pCO_2 (pCO_2(underway)) made by a continuous flow equilibration system (see for example Körtzinger et al., 1996 for a description of the method) in: October 2006, April, August, and October 2007, and April and October, 2008 on board the *CCGS Hudson*. The underway measurements were obtained on monitoring cruises on the Scotian Shelf (see Shadwick et al., 2011 for details of the field program). Measurements of pCO_2(underway) were made by a non-dispersive, infrared spectrometer (LiCor, LI-7000). The system was located in

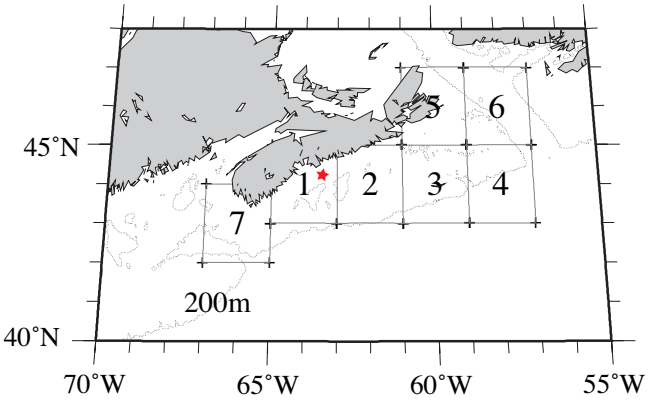

Fig. 4. The investigation is extrapolated spatially to include seven 2°×2° grid boxes covering the entire Scotian Shelf region (222 700 km^2). The CARIOCA buoy (red star) was moored at 44.3° N, 63.3° W, within grid box 1. Wind speed measurements were made at the Sable Island Meteorological Station at 43.9° N and 60.3° W, within grid box 3. The areas of each of the grid boxes (in km^2) are: box 1: 28470.29; box 2: 34653.14; box 4: 35527.77; box 5: 21500.94; box 6: 34308.70; and box 7: 32698.35.

the aft-laboratory of the ship and the intake depth was approximately 3 m below the water surface. Measurements were made every minute and used to compute hourly averages. The system was calibrated daily with both a CO_2-free reference gas (N_2) and a CO_2 calibration gas (328.99 ppm) provided by the US National Oceanic and Atmospheric Administration (NOAA). The data were corrected to in-situ water temperature and to 100% humidity and had an associated uncertainty of less than 1µatm. On the same cruises, discrete seawater samples were collected at the surface (depths of 3 or 5 m) and concentrations of dissolved inorganic carbon (DIC) and total alkalinity (TA) were measured (see Shadwick et al., 2011 for details). The DIC and TA measurements had an uncertainty of less than 2 and 3 µmol kg^{-1}, respectively. Following the determination of DIC and TA, discrete values of pCO_2 (pCO_2(DIC,TA)), were computed, using the standard set of carbonate system equations, excluding nutrients, with the CO_2 Sys program of Lewis and Wallace (1998). We used the equilibrium constants of Mehrbach et al. (1973) refit by Dickson and Millero (1987). The calcium (Ca^{2+}) concentration was assumed to be conservative and calculated from salinity. The uncertainty associated with the pCO_2(DIC,TA) was 4 µatm.

The pCO_2(MLR) is further compared to available surface pCO_2 in the Scotian Shelf region from the CARINA data base (pCO_2(CARINA)) from May 2004 to April 2008 (Figs. 6, 7 and Table 3) (CARINA, 2009). The pCO_2(underway) and pCO_2(CARINA) data represent mean values within a given 2°×2° grid box over 12 to 36 h, depending on the length of time the ship spent in a given grid box during the cruise. The different timescales of the computed pCO_2(MLR) (monthly) and measured (daily)

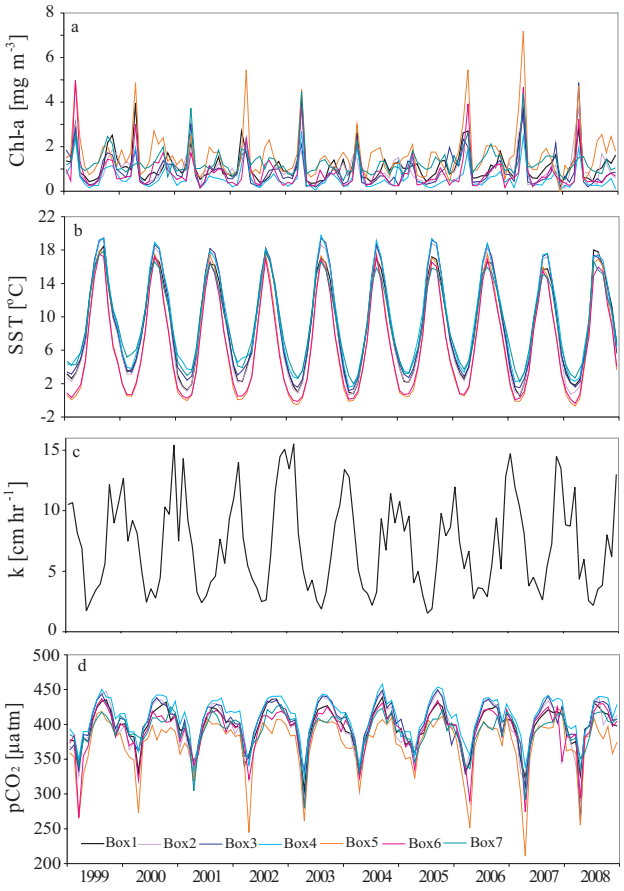

Fig. 5. Inputs used to compute the pCO_2 hindcast (pCO_2(MLR)): satellite derived **(a)** Chl_{SAT} and **(b)** SST, **(c)** gas transfer velocity (k) computed from hourly winds measured at Sable Island (Fig. 1) and **(d)** computed pCO_2(MLR), with grid boxes distinguished by color. For the locations of the grid boxes see Fig. 4.

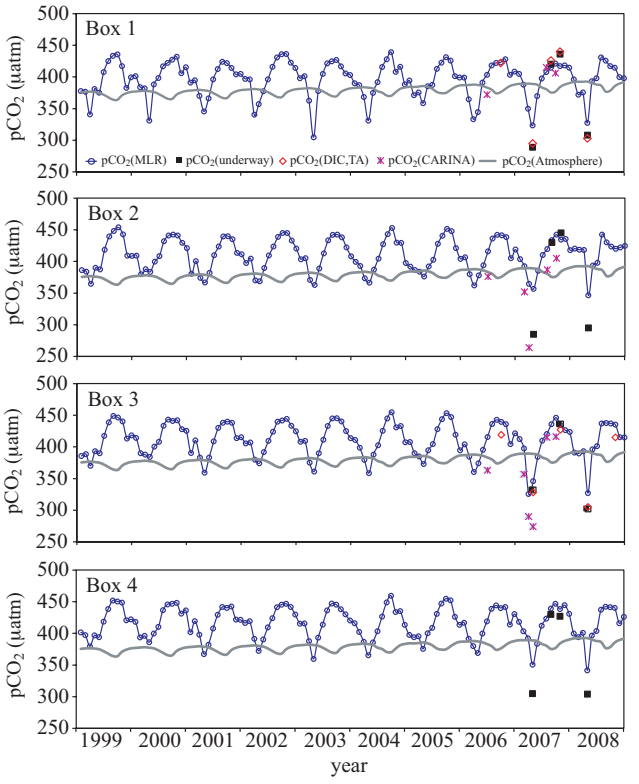

Fig. 6. The computed pCO_2(MLR) (blue line with symbols) is validated against three independent time-series of observations: pCO_2(underway), pCO_2(DIC,TA) and pCO_2(CARINA) in grid boxes 1 through 4. For the locations of the grid boxes see Fig. 4.

pCO_2(underway), pCO_2(DIC,TA), and pCO_2(CARINA) hinder a direct comparison. However, the agreement between the observed and computed pCO_2 supports the spatial extrapolation of the regression (Eq. 2). The pCO_2(MLR) overestimates the April pCO_2(CARIOCA) in both 2007 and 2008 (Fig. 8). The pCO_2(CARIOCA) is an average of hourly values at a point location over one month. The computed pCO_2(MLR) relies on Chl_{SAT} that has been both spatially and temporally averaged, which may explain the discrepancy between the peak values, seen for example, in April. A ten-year time series of discrete Chl-*a* measurements from the mooring location (not shown) indicates much higher concentrations than the Chl_{SAT} time-series used to predict pCO_2(MLR). However, these data are not monthly mean values, but once-per-month measurements that are expressly biased to produce snapshots of the dominant features of the system, most notably the spring Chl-*a* maximum, corresponding to the annual pCO_2 minimum. The April cruise on the Scotian Shelf is similarly biased; sampling takes place at the height of the spring bloom. The computed pCO_2(MLR) represents a monthly average, and the peak values are thus smoothed compared to the short-term ship-board observations. The computed pCO_2 reproduces very well the regional summer and autumn concentrations. Furthermore, there is good agreement between the pCO_2(MLR), pCO_2(underway), pCO_2(DIC,TA), and pCO_2(CARINA) outside of the spring bloom period in all grid boxes (Figs. 6, 7, Table 3).

4.4 Seasonal and interannual variability of pCO_2

On the Scotian Shelf the spring bloom occurs at the SST minimum allowing the effects of temperature and biology to be clearly distinguished (Shadwick et al., 2011a). The annual cycle of pCO_2 on the Scotian Shelf is dominated by the large seasonal amplitude of SST (Fig. 8a), with near 0 °C winter minimum, and summer maximum approaching 20 °C. The rapid and pronounced pCO_2 draw-down by the spring phytoplankton bloom in March or April is short-lived. The post-bloom recovery of pCO_2 is coincident with the warming of the surface waters, which acts to increase pCO_2. In autumn and winter, the deepening of the mixed layer facilitates intrusion of CO_2-rich waters into the surface layer and damps the decrease of pCO_2 due to the cooling of surface

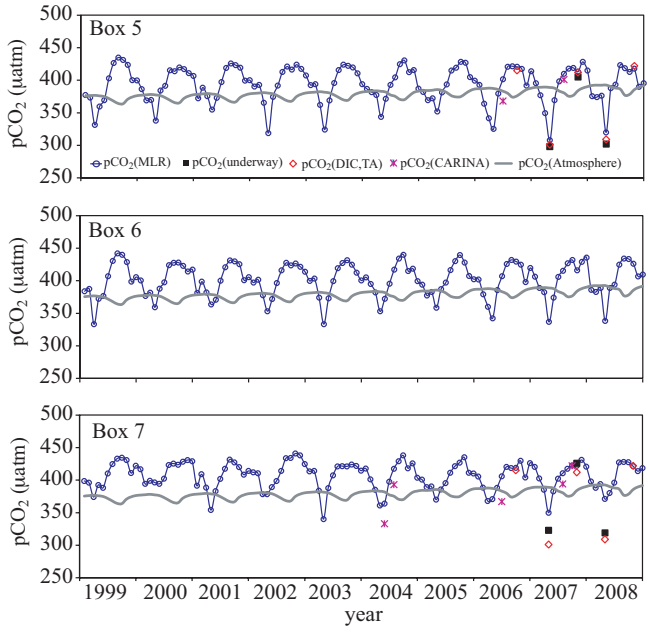

Fig. 7. The computed pCO_2 (MLR) (blue line with symbols) is validated against three independent time-series of observations: pCO_2(underway), pCO_2(DIC,TA) and pCO_2(CARINA) in grid boxes 5, 6 and 7. For the locations of the grid boxes see Fig. 4.

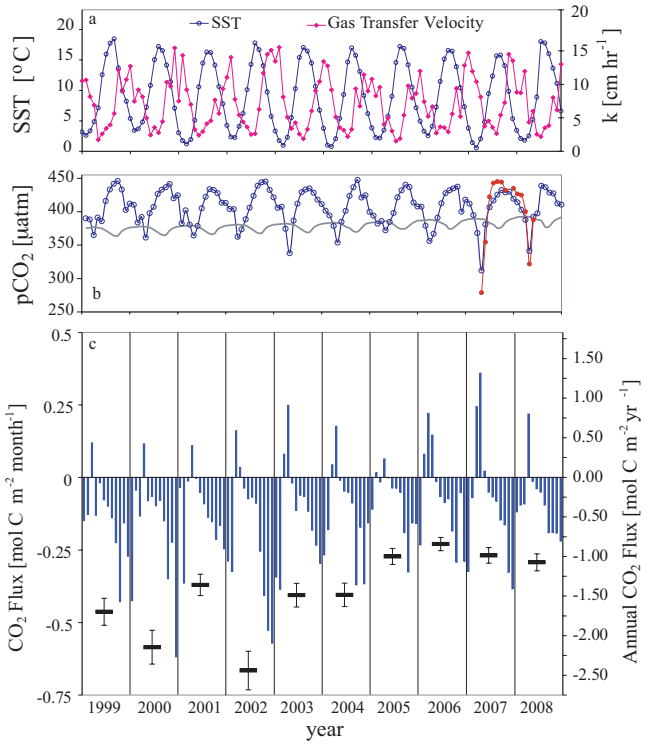

Fig. 8. (a) SST (blue line open symbols) and gas transfer velocity (pink line, closed symbols) for the 10-year period. **(b)** Computed pCO_2(MLR) for grid box 1 (see Fig. 4) comprising the mooring station (thick blue line with symbols). The computed pCO_2(MLR) has a standard error of 13 µatm. The CARIOCA pCO_2 used in the MLR are plotted in red. The solid gray line gives the monthly atmospheric CO_2 concentration. **(c)** The monthly CO_2 fluxes (vertical lines, left hand side y-axis) and integrated annual CO_2 fluxes (horizontal lines, right hand side y-axis) with an estimated 20% error.

waters. Overall, the surface waters of the Scotian Shelf act as a source of CO_2 to the atmosphere throughout most of the year (Fig. 8b). A reversal of this trend generally occurs only during, and immediately following, the spring phytoplankton bloom when the waters are undersaturated with respect to the atmosphere (Fig. 8b, c).

The overall direction and inter-annual variability of the annual CO_2 fluxes are preconditioned by temperature and wind speed in the winter and, less significantly, in the late summer and autumn. This occurs primarily through the control of the depth of the winter mixed-layer, and thus the availability of nutrients to fuel the spring bloom (Greenan et al., 2008). A more detailed investigation of the years 2002, 2003 and 2005 serves to illustrate the governing mechanisms (see also Fig. 8). The winter of 2001/2002 had warmer minimum temperatures, and weaker winds than the 10-year average. This permitted an early onset of stratification, and the initiation of the spring bloom beginning in March. Since mixing the previous winter was shallow, the bloom was inferred to be weak due to the reduced availability of nutrients from deeper waters. Following the weak bloom, strong late summer and autumn winds enhanced out-gassing in the second half of the year and yielded a large annual CO_2 flux to the atmosphere during 2002 (Fig. 8c). The winter of 2002/2003 had, in contrast, particularly cold minimum temperatures and strong winds resulting in deep mixing; the 2003 spring bloom was therefore pre-conditioned with high nutrient concentrations which is reflected in the magnitude of the CO_2 uptake in March and April, and the reduction in annual CO_2 release to the atmosphere relative to the previous year. It is not only the winter conditions that control the expression of the spring bloom. For example, a comparably weak wind regime during spring 2005 permitted the bloom and the CO_2 undersaturation of the surface waters to persist from February through May. In addition, cold summer maximum temperature and weak autumn winds inhibited outgassing in the second half of the year, and resulted in weak CO_2 release during 2005 (Fig. 8).

4.5 Multi-annual variability

The 10-year hindcast of pCO_2 and air-sea CO_2 fluxes reveals multi-annual to decadal trends in addition to the interannual variability (Fig. 8c). The mean seasonal cycles of SST and pCO_2 were computed using the mean value for each month over the ten-year period (i.e. mean of all January values, mean of all February values, etc). The SST and ΔpCO_2 anomalies were defined as the deviation from the mean seasonal cycle. The SST anomaly reveals a decrease of 0.13 °C per year, or 1.3 °C over the 10-year period of

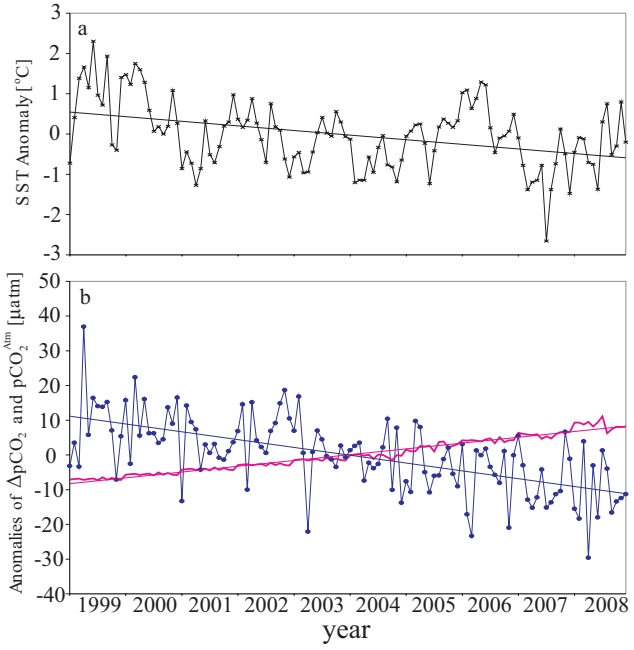

Fig. 9. Anomalies of **(a)** SST, and **(b)** ΔpCO_2 (blue circles) and atmospheric pCO_2 (pink solid line) within grid box 1 (see Fig. 4). The slope of SST linear regression line (solid black line) corresponds to a cooling of roughly 1.3 °C yr^{-1}. The slope of the atmospheric CO_2 anomaly (bold pink line) is roughly 1.7 µatm yr^{-1}, in line with the predicted annual increase due to anthropogenic emissions. The slope of the ΔpCO_2 anomaly (solid blue line) is −2.3 µatm yr^{-1}, or −23 µatm over the decade.

computation (Fig. 9). Simultaneously, the ΔpCO_2 ($\Delta pCO_2 = pCO_2^{Ocean} - pCO_2^{Atm}$), in which the anthropogenic atmospheric CO_2 increase has been explicitly included (Eqs. 2 and 3), decreased by 2.3 µatm per year, or 23 µatm over the decade (Fig. 9). This decrease in the ΔpCO_2 anomaly can satisfactorily be explained by the observed temperature decrease. The thermodynamic temperature correction for pCO_2 results in a 4% change in pCO_2 for a 1 °C change in temperature (Takahashi et al., 2002). Applying this correction to the decadal mean pCO_2 (roughly 420 µatm), the observed decrease in temperature anomaly (0.13 °C per year) would account for a decrease in ΔpCO_2 of 2.2 µatm per year, as revealed by the ΔpCO_2 anomaly. The negative, or near neutral, North Atlantic Oscillation (NAO) index over the past decade is associated with an increased transport of cold Labrador Current Water onto the Scotian Shelf, and thus with anomalously cold waters in the region (Thompson and Wallace, 2001; Petrie, 2007; Thomas et al., 2008). The cooling of the water effectively shifts the position of the equilibrium ΔpCO_2 state, driving the system toward uptake. Conversely, warming of the water drives the system toward outgassing. Thus, while the interannual variability is controlled by local atmospheric forcing, the multi-annual to decadal changes appear to be influenced by larger scale hemispheric processes, in this case represented by the local expression of the NAO.

4.6 Shelf-wide CO_2 fluxes

The satellite-based extrapolation of the pCO_2 algorithm to include the wider Scotian Shelf region allows the spatial variability in the region to be assessed (Figs. 10 to 13). From 1999–2008, the shelf integrated fluxes vary substantially between −1.7 mol C m^{-2} yr^{-1} (or −380 Gmol C yr^{-1}, over the shelf area) and −0.02 mol C m^{-2} yr^{-1} (or −3.9 Gmol C yr^{-1}, over the shelf area, see also Fig. 13 and Table 4). A gradient exists between the northern Cabot Strait, and the southwestern region in the Gulf of Maine (Fig. 1). The Cabot Strait region has consistently weaker annual CO_2 release, and even acts in some years as a sink for CO_2. The Cabot Strait region (grid boxes 5 and 6) exhibited the coldest (below 0 °C) winter temperatures due to the outflow of water from the seasonally ice-covered Gulf St. Lawrence (Fig. 11). The highest values of Chl_{SAT} were also observed in grid boxes 5 and 6, resulting in the strongest spring blooms and corresponding to the largest seasonal CO_2 uptake during the year (Figs. 5, 10 and 13). In contrast, the Gulf of Maine (grid box 7), under greater influence of the Gulf Stream and lesser influence of the Labrador Current, is warmer (Fig. 11). In the Gulf of Maine region, the spring bloom, and corresponding CO_2 uptake, is weaker (Fig. 13). Both the Cabot Strait and Gulf of Maine regions exhibit large post-bloom Chl_{SAT} (Fig. 5) relative to the central Scotian Shelf (boxes 1 to 4). The central Scotian Shelf region also exhibits the warmest summer temperatures, and the largest CO_2 outgassing in summer and autumn (Fig. 5). There is a north-south gradient in the annual mean pCO_2 (Fig. 12) with the lowest mean values observed in the Cabot Strait region and increasing southward with relatively higher annual mean pCO_2 in the Gulf of Maine. There is also a gradient between the offshore and coastal regions, with lower pCO_2, colder temperatures, and higher Chl_{SAT} concentrations in the near-shore grid boxes relative to the grid boxes further offshore (Fig. 10). While a particularly large CO_2 release is computed for the years 2000 and 2002 over the whole region (see also Fig. 8c), the general trend for the 10-year period is a weakening CO_2 release consistent with the decreasing trend in the ΔpCO_2 anomaly over the shelf (Fig. 9). The gradual change toward stronger CO_2 uptake on the Scotian shelf is in line with interpretations of the role of the NAO in controlling hydrographic patterns (Schuster and Watson, 2007; Thomas et al., 2008; Ullman et al., 2009). However, consistent with suggestions of a longer-term decline in the CO_2 sink in the North Atlantic Ocean as a whole (Watson et al., 2009; Metzl et al., 2010), we cannot presently exclude the possibility that long-term changes in North Atlantic circulation patterns would potentially cause similar trends due to a weakened northward, and strengthened southward, water transport (Bryden et al., 2005).

This approach to understand the dynamics of the CO_2 system on the Scotian Shelf and a recent observation-based approach (Shadwick et al., 2011a) yield conflicting results to modelling studies of the same region which suggest that the

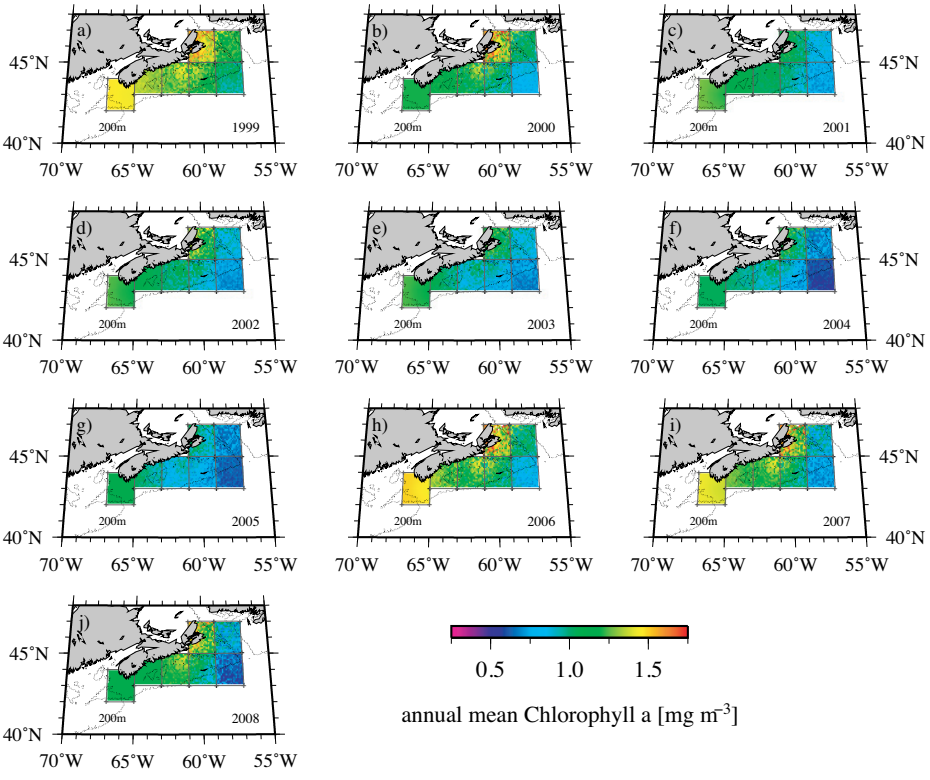

Fig. 10. The annual mean satellite derived Chl_{SAT} from 1999 (top left) to 2008 (bottom left).

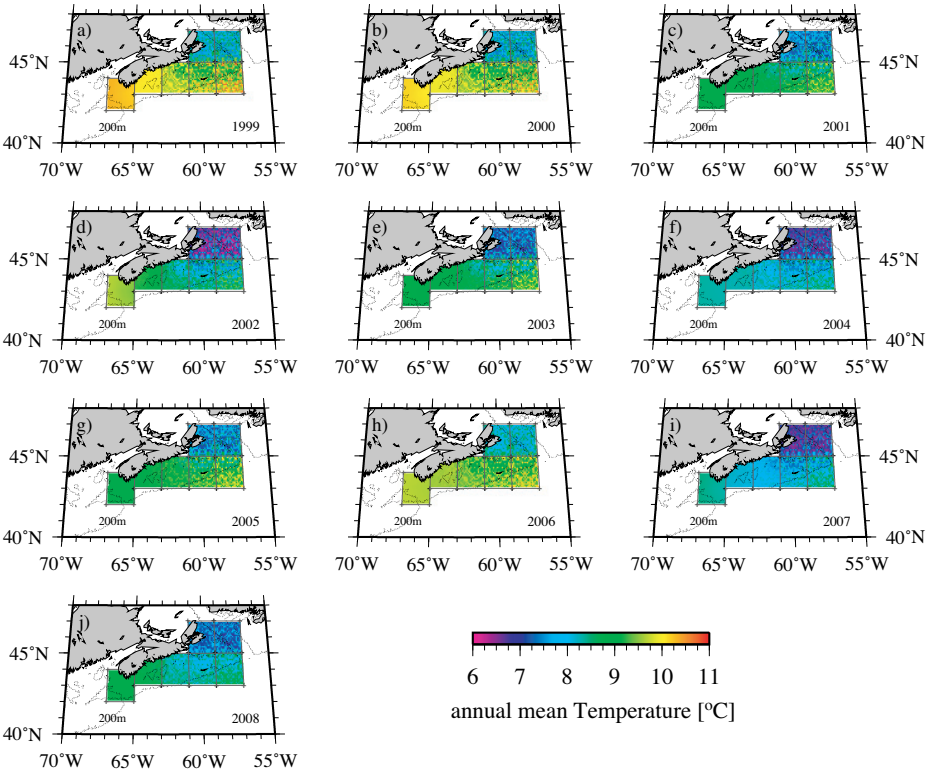

Fig. 11. The annual mean satellite derived SST from 1999 (top left) to 2008 (bottom left).

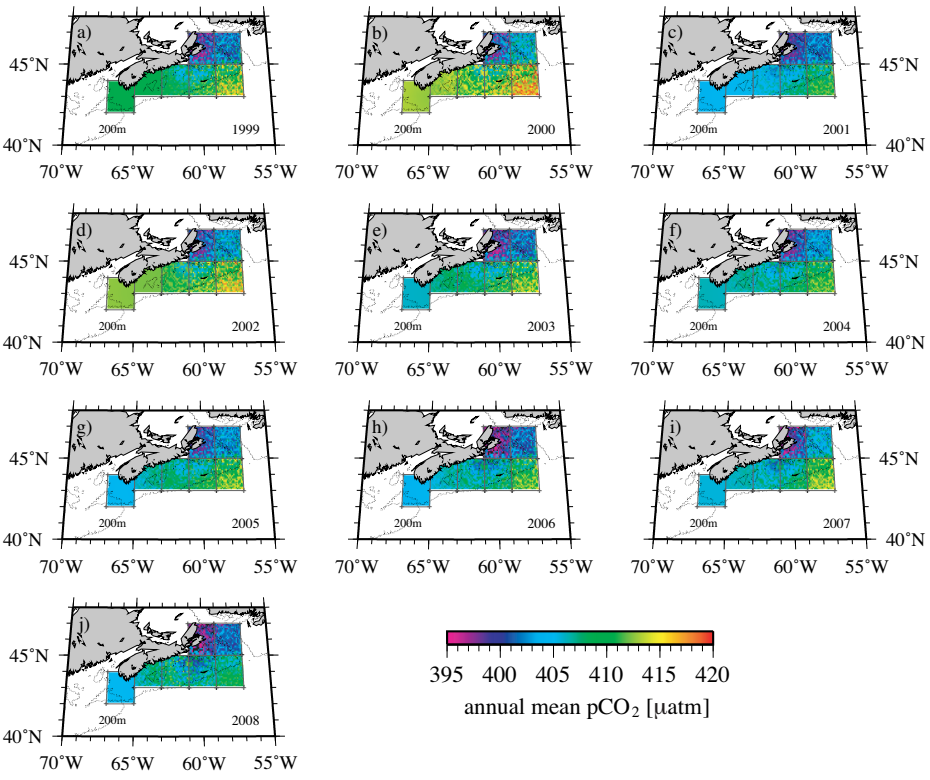

Fig. 12. The annual mean pCO_2(MLR) computed from satellite derived Chl_{SAT} and SST, and the gas transfer velocity (estimated from winds measured at Sable Island) using Eq. (2), from 1999 (top left) to 2008 (bottom left).

Scotian Shelf acts as a sink for atmospheric CO_2 annually (Fennel et al., 2008; Previdi et al., 2009). However, our observations are in agreement with those of similar process studies in the neighboring Gulf of Maine (Salisbury et al., 2009; Shadwick et al., 2011a; Vandemark et al., 2010). Previdi et al. (2009) have suggested that interannual variability in air-sea CO_2 flux on the eastern North American continental shelf is due in part to NAO forcing. They suggest that warming between (low NAO) 1985 and (high NAO) 1990 drove the system in the Gulf of Maine towards weaker uptake; this interpretation is agreement with our finding that the decadal cooling on the Scotian Shelf has driven the system towards stronger uptake. The reasons for the discrepancy between the observation- and model-based approaches is currently unknown and is beyond the scope of this study.

5 Discussion

5.1 The Scotian Shelf in the larger global context

Our findings indicate that the Scotian Shelf acts a source of CO_2, contrary to findings in many high-latitude continental shelf seas that act as net sinks for atmospheric CO_2 (Thomas et al., 2004; Chen and Borges, 2009). The East China Sea, an example of a continental shelf sea in the western Pacific, is similar to the Scotian Shelf with respect to its location on the western side of the ocean basin under the influence of a warm northward flowing boundary current. Hydrography on the Scotian Shelf is additionally influenced by the southward flow of the cold Labrador Current; these waters warm significantly as they transit, increasing the pCO_2 and contributing to the outgassing in the region. The East China Sea has been well studied with respect to the inorganic carbon system (e.g. Tsunogai et al., 1997; Chen and Wang, 1999; Tsunogai et al., 1999; Wang et al., 2000). The East China Sea absorbs roughly twice as much CO_2 as is emitted annually from the Scotian Shelf region. The outgassing of CO_2 on the Scotian Shelf is primarily due to the competing effects of temperature and biology in the system, along with the late-autumn and winter destratification of the water column. The spring bloom on the Scotian Shelf results in a significant but brief CO_2 draw down, and occurs at the temperature minimum. The decay of this bloom, and resulting production of CO_2 through the remineralization of organic matter is coincident with surface warming, which increases the pCO_2 to supersaturation with respect to the atmosphere. C biological production in the summer and early autumn is not sufficient to overcome this supersaturation. The water cools in late autumn, reducing pCO_2. Over the same period the water column becomes destratified maintaining the surface supersaturation until the following spring. The Scotian Shelf behaves similarly to an upwelling system, which are

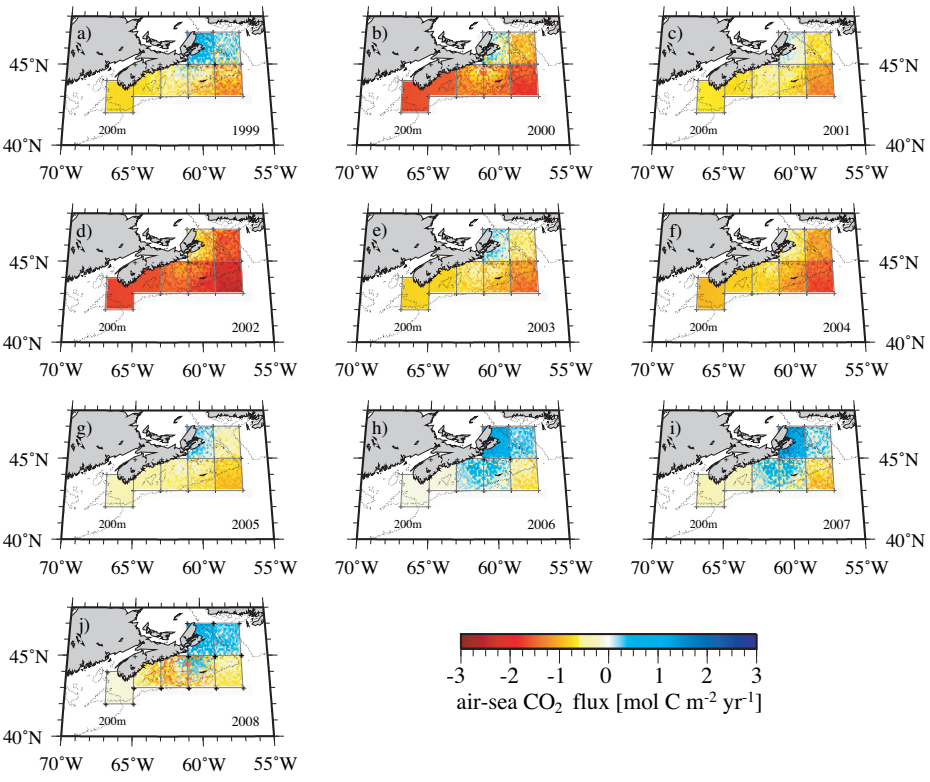

Fig. 13. The investigation is extrapolated spatially to include the entire Scotian Shelf region (222 700 km^2). The integrated annual air-sea CO_2 fluxes from 1999 (top left) to 2008 (bottom left) are shown. The annual, shelf-wide fluxes are: **(a)**, -0.6 mol C m^{-2} yr^{-1} (1999), **(b)** -1.3 mol C m^{-2} yr^{-1} (2000), **(c),** -0.7 mol C m^{-2} yr^{-1} (2001), **(d)** -1.7 mol C m^{-2} yr^{-1} (2002), **(e)** -0.8 mol C m^{-2} yr^{-1} (2003), **(f)** -1.1 mol C m^{-2} yr^{-1} (2004), **(g)** -0.5 mol C m^{-2} yr^{-1} (2005), **(h)** -0.02 mol C m^{-2} yr^{-1} (2006), **(i)** -0.1 mol C m^{-2} yr^{-1} (2007) and **(j)** -0.1 mol C m^{-2} yr^{-1} (2008). Negative values indicate CO_2 release to the atmosphere.

Table 4. The annual air-sea CO_2 fluxes from 1999 to 2008, both shelf-wide, and in grid box 1 comprising the CARIOCA mooring, in units of mol C m^{-2} yr^{-1}. Negative values indicate an outgassing of CO_2 to the atmosphere. The 7 grid boxes covering the Scotian Shelf region have an area of 222 700 km^2; Box 1 has an area of 31 800 km^2 (see also Fig. 13).

	1999	2000	2001	2002	2003	2004	2005	2006	2007	2008
Shelf-wide	−0.6	−1.3	−0.7	−1.7	−0.8	−1.1	−0.5	−0.02	−0.1	−0.1
Box 1	−1.75	−2.25	−1.4	−2.45	−1.5	−1.5	−1.0	−0.8	−0.95	−1.1

often biologically productive systems which release CO_2 to the atmosphere due to the delivery of DIC-rich waters from below (Lendt et al., 2003; Thomas et al., 2005). By contrast, the North Sea, which acts a sink for atmospheric CO_2 of roughly the same magnitude as the Scotian Shelf source (Thomas et al., 2005), could be classified as a downwelling system (Huthnance et al., 2009). It has been suggested that the downwelling circulation in the North Sea promotes the transport of dissolved inorganic carbon off the shelf to the deep ocean facilitating the uptake of atmospheric CO_2 in the subsequent productive season (Huthnance et al., 2009).

The physical system on the Scotian Shelf may alternatively be thought of as estuarine; there is an inflow of deep, nutrient- and carbon-rich water and an outflow of nutrient-deplete surface waters. By contrast, Amundsen Gulf, in the southwestern region of the Canadian Arctic Archipelago, which exports subsurface water to the Beaufort Sea (Lanos, 2009; Shadwick et al., 2011b) may be thought of as an anti-estuarine system; there is an outflow (to the Beaufort Sea) of carbon- and nutrient-rich subsurface waters, and an inflow (from the Beaufort Sea) of nutrient-poor surface waters (Lanos, 2009). The Amundsen Gulf system may also be considered downwelling system, like the North Sea, in which the transport of carbon-rich subsurface waters from the Gulf

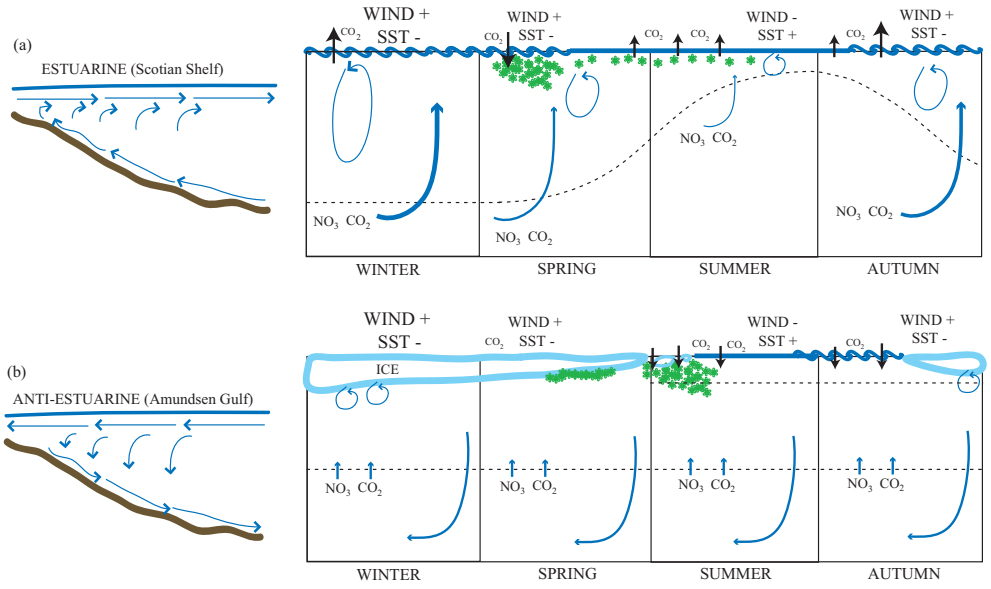

Fig. 14. A schematic representation of the systems in **(a)** the Scotian Shelf and **(b)** Amundsen Gulf. The Scotian Shelf may be thought of as an estuarine system; subsurface waters are delivered to the surface by a combination of wind mixing, upwelling and convection (blue arrows). The mixed-layer depth is represented by the dashed line. In contrast, Amundsen Gulf may be thought of as an anti-estuarine, or downwelling, system. Wind and convective mixing are inhibited by ice-cover in winter and nutrient-rich waters are delivered to the surface layer primarily by diffusive processes. Density driven mixing by the release of brine during sea-ice formation makes a contribution in the autumn and winter (blue arrows). The mixed-layer depth is roughly 50 m (dashed line) throughout the year; strong surface stratification in the upper 10–20 m is observed following sea-ice melt.

facilitates the uptake of atmospheric CO_2 in the subsequent productive season (Shadwick et al., 2011b). The two systems are shown schematically in Fig. 14. In both cases, a portion of the surface DIC lost due to biological production is balanced over the annual cycle by inputs of DIC from below (Shadwick et al., 2011a,b). As described above, in the case of the Scotian Shelf, this carbon-rich water is brought to the surface in the autumn and winter by a combination of wind, upwelling and convective mixing. In Amundsen Gulf, the water column is strongly stratified throughout the year, and nutrients and inorganic carbon are brought to the surface either in the brief ice-free period in autumn when storms increase and the region is subject to wind mixing, or by diffusive mixing throughout the year. In general, however, vertical input of DIC- and nutrient- rich waters is inhibited by the downwelling, or anti-estuarine circulation. Furthermore, sea-ice cover in winter prevents the convective mixing seen on the Scotian Shelf as a result of heat loss from the surface ocean to the atmosphere. During the majority of the open water season in Amundsen Gulf the surface waters, and air-temperatures, are relatively warm. The remainder of the DIC lost to biological production in Amundsen Gulf is resupplied by the uptake of atmospheric CO_2 during the open water season (Fig. 14) (Shadwick et al., 2011b). Under this upwelling (estuarine) or downwelling (anti-estuarine) characterization, the source or sink status with respect to atmospheric CO_2 of both the Scotian Shelf and Amundsen Gulf systems complement the synthesis of Chen and Borges (2009) and the most recent climatology of Takahashi et al. (2009) with respect to coastal ocean systems.

6 Conclusions

High frequency in-situ time-series observations deepen our understanding of individual regional characteristics of the CO_2 system particularly in coastal regions, where temporal and spatial variability is high. This allows reliable relationships between pCO_2 and remotely sensed variables to be established and understood. Coupled to such in-situ observations, the application of satellite data has the potential to improve the understanding and assessment of air-sea CO_2 fluxes in the coastal ocean, which, as shown here, can vary by two orders of magnitude at interannual to decadal times scales.

Appendix A

Interpretation of the SST regression coefficient

A detailed analysis of the time series, paying particular attention to the relationship between pCO_2 and SST, in the frequency domain facilitates an understanding of the deviation of the temperature coefficient (4.6 µatm $(°C)^{-1}$) in

the regression (Eq. (2) in the main text) from the expected thermodynamic value. Using a frequency analysis (e.g. Shumway and Stoffer, 2006), we decomposed the temperature coefficient into genuine thermodynamic temperature effects, and effects with timing correlated to temperature, which are also encompassed by the SST coefficient.

We computed the cross-spectrum of pCO_2 and SST in order to examine the strength of the relationship between these two parameters over a range of frequencies (Shumway and Stoffer, 2006); the gain in pCO_2 due to SST is plotted in Fig. A1a (in blue). The dominant energies in the pCO_2-temperature relationship are found at frequencies, f, $\leq 0.04\,\mathrm{hr}^{-1}$, and corresponding to periods of P$\geq$24-h. At the daily frequency, $f = 0.04\,\mathrm{hr}^{-1}$, (highlighted by pale blue vertical bar in Fig. A1a), the gain has a value of approximately 16 µatm $(°C)^{-1}$, which is what the thermodynamic relationship between pCO_2 and temperature predicts (a 4% change in pCO_2 for a 1 °C change in temperature (Takahashi et al., 2002), with a mean annual pCO_2 of roughly 400 µatm). Mechanistically, this is caused by the fact that the seasonal variability of temperature on the Scotian Shelf is primarily driven by surface heat fluxes (Umoh and Thompson, 1994), reflected here by the dominance of SST controlling the daily variability in pCO_2. At frequencies less than $f = 0.04\,\mathrm{hr}^{-1}$, or for periods longer than 24-h, the temperature related gain in pCO_2 tends away from the thermodynamic value, towards the lower value (4.6 µatm $(°C)^{-1}$) obtained in the regression presented here (Eq. (2) in the main text).

To evaluate the effects correlated with temperature outside of the diurnal cycle, the daily, or 24-h, cycle was removed from the SST time series. This was done by computing the mean temperature over a given, discrete 24-h period, starting at midnight, and subtracting this value from each hourly value of SST over the same period:

$$\mathrm{SST}_{(\mathrm{in-situ})} - \mathrm{SST}_{(\mathrm{daily\ mean})} = \Delta\mathrm{SST}^{*} \qquad \text{(A1)}$$

This daily cycle in SST was subsequently removed from the pCO_2 time series via the following equation:

$$pCO_2{}^{*} = pCO_2 - (pCO_2[\exp(0.0423\Delta\mathrm{SST}^{*})]) \qquad \text{(A2)}$$

where the second term on right-hand side of the equation is the temperature correction of Takahashi et al. (2002), and the superscript "*" indicates the time series with the 24-h cycle removed.

The gain in pCO_2* due to SST* is shown in Fig. A1a (red dashed line). The energy of the daily frequency has vanished to a large degree ($f = 0.04\,\mathrm{hr}^{-1}$, highlighted by the pale blue vertical bars in Fig. A1), and the temperature correlated pCO_2* gain at $f = 0.02\,\mathrm{hr}^{-1}$, which correspond to periods shorter than 50 h, (highlighted by the pink vertical bars in Fig. A1), lies between 4 and 6 µatm $(°C)^{-1}$ which is consistent with the SST coefficient obtained in the regression (Eq. (2) in the main text). The dominant gain in the temperature corrected pCO_2 data however is now observed

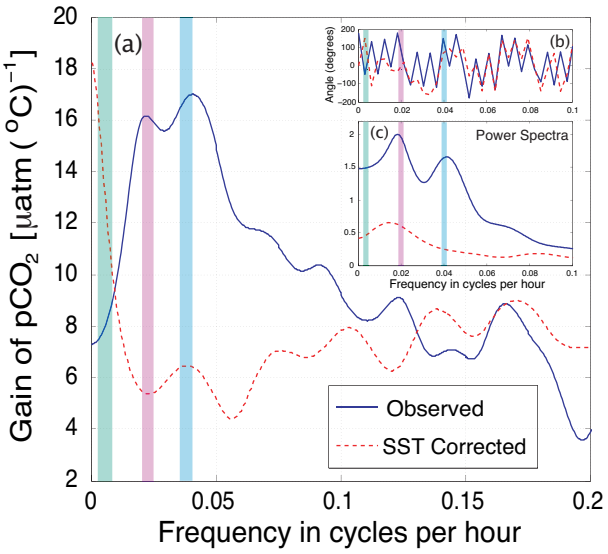

Fig. A1. (a) The gain of pCO_2 due to SST using the in-situ hourly data (blue), and the gain of pCO_2* due to SST* (red dashed). Frequencies of $f = 0.04\,\mathrm{hr}^{-1}$, or 24-h (blue bar), $f = 0.02\,\mathrm{hr}^{-1}$ or roughly 40 h (pink bar), and $f = 0.007\,\mathrm{hr}^{-1}$ or 6 days (green bar) are indicated. **(b)** The phase spectra for the in-situ pCO_2 (blue line) and pCO_2* (red dashed line) series. **(c)** The power spectra for the in-situ pCO_2 (blue) and pCO_2* series (red dashed). The in-situ data is dominated by the 24-h cycle of SST, while the pCO_2* series is dominated over longer time scales

at a frequency of $f = 0.007\,\mathrm{hr}^{-1}$, (highlighted by the green vertical bars in Fig. A1), corresponding to periods from several days to a month. The gain at this frequency is 13 µatm $(°C)^{-1}$, with a phase lag of roughly 180 degrees (highlighted by the green vertical bars in Fig. A1b), or -13 µatm $(°C)^{-1}$, and can be attributed to biological CO_2 uptake, with seasonal cycle strongly anti-correlated to that of temperature. This anti-correlation has been confirmed by Shadwick et al. (2011a), by employing an alternate 1-D modelling approach. Furthermore, a linear regression of the temperature corrected pCO_2 data with in-situ temperature, as shown by Shadwick et al. (2011a) (their Fig. 8), yields a coefficient of -13 µatm $(°C)^{-1}$, as described above. For frequencies shorter than $f = 0.007\,\mathrm{hr}^{-1}$, (periods longer than 6 days), the gain in pCO_2 due to SST in the in-situ data (Fig. A1, blue line) approaches the value of 4.6 µatm $(°C)^{-1}$ obtained with the regression.

Acknowledgements. We thank R. Davis for his assistance with the CARIOCA data processing, K. Thompson and J. Cullen for assistance with the statistical analysis and in-depth comments on the manuscript, and D. Worthy at Environment Canada for providing the atmospheric CO_2 data. We are grateful to J. Barthelotte, M. Scotney, and B. Greenan for the deployment and recovery of the CARIOCA buoy, and to J. Spry and the Bedford Institute of Oceanography for making the archived data from station HL2 accessible. We wish to thank Nick Bates and three anonymous reviewers for their constructive comments that have considerably improved the manuscript. This work was supported by the National Science and Engineering Research Council of Canada, the Canadian Foundation for Climate and Atmospheric Sciences, the National Science Foundation, NASA, and by MetOcean Data Systems. This work contributes to IGPB/IHDP-LOICZ.

Edited by: A. V. Borges

References

Bakker, D. C. E., Etcheto, J., Boutin, J., and Merlivat, L.: Variability of surface water fCO_2 during seasonal upwelling in the equatorial Atlantic Ocean as observed by a drifting buoy, J. Geophys. Res., 106, 9241–9253, 2001.

Banse, K.: Zooplankton: Pivotal role in the control of ocean production, J. Mar. Sci., 52, 265–277, 1995.

Bates, N. R., Merlivat, L., Beaumont, L., and Pequignet, A. C.: Intercomparison of shipboard and moored CARIOCA buoy seawater fCO_2 measurements in the Sargasso Sea, Mar. Chem., 72, 239–255, 2000.

Bigelow, H. B.: Physical Oceanography of the Gulf of Maine, Bull. U.S. Bur. Fish., 640, 511–1027, 1927.

Borges, A. V.: Do We Have Enough Pieces of the Jigsaw to Integrate CO_2 Fluxes in the Coastal Ocean?, Estuaries, 28, 3–27, 2005.

Borges, A. V., Delille, B., and Frankignoulle, M.: Budgeting sinks and sources of CO_2 in the coastal ocean: Diversity of ecosystems counts, Geophys. Res. Lett., 32, L14601, doi:10.1029/2005GL023053, 2005.

Borges, A. V., Tilbrook, B., Metzl, N., Lenton, A., and Delille, B.: Inter-annual variability of the carbon dioxide oceanic sink south of Tasmania, Biogeosciences, 5, 141–155, doi:10.5194/bg-5-141-2008, 2008.

Boutin, J. and Merlivat, L.: New in-situ estimates of carbon biological production rates in the Southern Ocean from CARIOCA drifter measurements, Geophys. Res. Lett., 36, L13608, doi:10.1029/2009GL038307, 2009.

Bryden, H. L., Longworth, H. R., and Cunningham, S. A.: Slowing of the Atlantic meridional overturning circulation at 25°N, Nature, 438, 655–657, 2005.

Cai, W.-J., Dai, M. H., and Wang, H. C.: Air-sea exchange of carbon dioxide in ocean margins: A province-based synthesis, Geophys. Res. Lett., 33, L12603, doi:10.1029/2006GL026219, 2006.

CARINA: Carbon in the Atlantic Ocean Region - the CARINA project: Results and Data, Version 1.0, Tech. rep., Carbon Dioxide Information Analysis Center, Oak Ridge National Laboratory, U.S. Department of Energy, Oak Ridge, TN, USA, doi: 10.3334/CDIAC/otg.CARINA.ATL.V1.0, 2009.

Chapman, D. C. and Beardsley, R. C.: On the origin of shelf water in the Middle Atlantic Bight, J. Phys. Oceanogr., 19, 384–391, 1989.

Chen, C.-T. A. and Borges, A. V.: Reconciling opposing views on carbon cycling in the coastal ocean: Continental shelves as sinks and near-shore ecosystems as sources of atmospheric CO_2, Deep-Sea Res. Pt. II, 33, L12603, doi:10.1016/j.dsr2.2009.01.001, 2009.

Chen, C. T.-A. and Wang, S. L.: Carbon, alkalinity and nutrient budget on the East China Sea continental shelf, J. Geopys. Res., 104, 20675–20686, 1999.

Chierici, M., Olsen, A., Johannessen, T., Trinanes, J., and Wanninkhof, R.: Algorithms to estimate the carbon dioxide uptake in the northern North Atlantic using shipboard observations, satellite and ocean analysis data, Deep-Sea Res., 56, 630–639, 2009.

Copin-Montégut, C., Bégovic, M., and Merlivat, L.: Variability of the partial pressure of CO_2 on diel to annual time scales in the northwestern Mediterranean Sea, Mar. Chem., 85, 169–189, 2004.

Dickson, A. G. and Millero, F. J.: A comparison of the equilibrium constants for the dissociation of carbonic acid in seawater media, Deep-Sea Res. Pt. II, 34, 1733–1743, 1987.

Donohue, S.: A numerical model of an upwelling event off the coast of Nova Scotia, Master's thesis, Royal Military College of Canada, 2000.

Etcheto, J., Boutin, J., Dandonneau, Y., Bakker, D. C. E., Feely, R. A., Ling, R. D., Nightingale, P. D., and Wanninkhof, R.: Air-sea CO_2 flux variablity in the equatorial Pacific Ocean near 100°W, Tellus B, 51, 734–737, 1999.

Fennel, K., Wilkin, J., Previdi, M., and Najjar, R.: Denitrification effects on air-sea CO_2 flux in the coastal ocean: Simulations for the northwest North Atlantic, Geophys. Res. Lett., 35, L24608, doi:10.1029/2008GL036147, 2008.

Greenan, B. J. W., Petrie, B. D., Harrison, W. G., and Oakey, N. S.: Are the spring and fall blooms on the Scotian Shelf related to short-term physical events?, Cont. Shelf Res., 24, 603–625, 2004.

Greenan, B. J. W., Petrie, B. D., Harrison, W. G., and Strain, P. M.: The Onset and Evolution of a Spring Bloom on the Scotian Shelf, Limnol. Oceanogr., 53, 1759, 2008.

Hachey, H. B.: The effect of a storm on an inshore area with markedly stratified waters, J. Bio. Board Can., 1, 227–237, 1935.

Hachey, H. B.: The waters of the Scotian Shelf, J. Fish. Res. Board Can., 5, 377–397, 1942.

Hannah, C. G., Shore, J. A., and Loder, J. W.: Seasonal Circulation on the Western and Central Scotian Shelf, J. Physical Oceanography, 31, 591–615, 2001.

Houghton, R. W. and Fairbanks, R. G.: Water Sources for Georges Bank, Deep-Sea Res. Pt. II, 48, 95–114, 2001.

Huthnance, J. M., Holt, J. T., and Wakelin, S. L.: Deep ocean exhange with west-European shelf seas, Ocean Sci., 5, 621–634, 2009, http://www.ocean-sci.net/5/621/2009/.

Khatiwala, S. P., Fairbanks, R. G., and Houghton, R. W.: Freshwater souces to the coastal ocean off northeastern North America: Evidence from $H_2^{18}O/H_2^{16}O$, J. Geophys. Res., 104, 18241–18255, 1999.

Kiefer, D. A.: Fluorescence Properties of Natural Phytoplankton Populations, Marine Biology, 22, 263–269, 1973.

Körtzinger, A., Thomas, H., Schneider, B., Gronau, N., Mintrop, L., and Duinker, J. C.: At-sea intercomparison of two newly designed underway pCO_2 systems – encouraging results, Mar. Chem., 52, 133–145, 1996.

Lanos, R.: Circulation Régionale, Masses d'Eau,Cycles d'Évolution et Transports Entre la Mer de Beaufort et le Golfe d'Amundsen, Ph.D. thesis, Univérsité du Québec, 2009.

Laruelle, G. G., Dürr, H. H., Slomp, C. P., and Borges, A. V.: Evaluation of sinks and sources of CO_2 in the global coastal ocean using a spatially-explicit typology of estuaries and continental shelves, Geophys. Res. Lett., 37, L15607, doi:10.1029/2010GL043691, 2010.

Lefèvre, N., Aiken, J., Rutllant, J., Daneri, G., Lavender, S., and Smyth, T.: Observations of pCO_2 in the coastal upwelling off Chile: Spatial and temporal extrapolation using satellite data, J. Geophys. Res., 107, 3055, doi:10.1029/2000JC000395, 2002.

Lefévre, N., Guillot, A., Beaumont, L., and Danguy, T.: Variability of fCO_2 in the Eastern Tropical Atlantic from a moored buoy, J. Geophys. Res., 113, C01015, doi:10.1029/2007JC004146, 2008.

Lendt, R., Thomas, H., Hupe, A., and Ittekkot, V.: Response of the near-surface carbonate system of the northwestern Arabian Sea to the southwest monsoon and related biological forcing, J. Geophys. Res., 108, 3222, doi:10.1029/2000JC000771l, 2003.

Levitus, S.: Climatological Atlas of the World Ocean, NOAA Professional Paper, 13, 1982.

Lewis, E. and Wallace, D. W. R.: Program Developed for CO_2 Systems Calculations, ORNL/CDIAC 105, Carbon Dioxide Information Analysis Center, Oak Ridge National Laboratory US Department of Energy, Oak Ridge, Tennessee, 1998.

Loder, J. W., Han, G., Hannah, C. G., Greenberg, D. A., and Smith, P. C.: Hydrography and baroclinic circulation in the Scotian Shelf region: winter versus summer, Can. J. Fish. Aquat. Sci., 54, 1997.

Loder, J. W., Petrie, B., and Gawarkiewicz, G.: The coastal ocean off northeastern North America: A large-scale view, in: The Sea, The Global Coastal Ocean: Regional Studies and Syntheses, John Wiley, New York, NY, USA, 1998.

Lohrenz, S. E. and Cai, W.-J.: Satellite ocean color assessment of air-sea fluxes of CO_2 in a river-dominated coastal margin, Geophys. Res. Lett., 33, L01 601, doi:10.1029/2005GL023942, 2006.

Mehrbach, C., Culberson, C. H., Hawley, J. E., and Pytkowicz, R. M.: Measurement of the apparent dissociation constants of carbonic acid in seawater at atmospheric pressure, Limnol. Oceangr., 18, 897–907, 1973.

Metzl, N., Corbière, A., Reverdin, G., Lenton, A., Takahashi, T., Olsen, A., Johannessen, T., Pierrot, D., Wanninkhof, R., Ólafsdóttir, S. R., Olafsson, J., and Ramonet, M.: Recent acceleration of the sea surface fCO_2 growth rate in the North Atlantic subpolar gyre (1993-2008) revealed by winter observations, Global Biogeochem. Cycles, 24, GB4004, doi:10.1029/2009GB003658, 2010.

Naegler, T., Ciais, P., Rodgers, K., and Levin, I.: Excess radiocarbon constraints on air-sea gas exchange and the uptake of CO_2 by the oceans, Geophys. Res. Lett., 33, L11802, doi:10.1029/2005GL025408L, 2006.

Nightingale, P. D., Malin, G., Law, C. S., Watson, A. J., Liss, P. S., Liddicoat, M. I., Boutin, J., and Upstill-Goddard, R. C.: In situ evaluation of the air-sea gas exchange parameterizations using novel conservative and volatile tracers, Global Biogeochemical Cycles, 14, 373–387, 2000.

Olsen, A., Brown, K. R., Chierici, M., Johannessen, T., and Neill, C.: Sea-surface CO_2 fugacity in the subpolar North Atlantic, Biogeosciences, 5, 535–547, doi:10.5194/bg-5-535-2008, 2008.

Padin, X. A., Castro, C. G., Rios, A. F., and Pérez, F. F.: fCO_2^{sw} variability in the Bay of Biscay during ECO cruises, Cont. Shelf Res., 28, 904–914, 2008.

Petrie, B.: Current Response at the Shelf Break to Transient Wind Forcing, J. Geophys. Res., 88, 9567–9578, 1983.

Petrie, B.: Does the North Atlantic Oscillation affect hydrographic properties on the Canadian Atlantic continental shelf?, Atmos.-Ocean, 45, 141–151, 2007.

Petrie, B. and Smith, P. C.: Low-frequency motions on the Scotian shelf and slope, Atmosphere, 15, 117–140, 1977.

Platt, T., Bird, D., and Sathyendranath, S.: Critical depth and marine primary production, Proc. R. Soc. London, Ser. B, 246, 205–217, 1991.

Previdi, M., Fennel, K., Wilkin, J., and Haidvogel, D.: Interannual variability in atmospheric CO_2 uptake on the northeast U.S. continental shelf, J. Geophys. Res., 114, G04003, doi:10.1029/2008JG000881, 2009.

Sabine, C. L., Feely, R. A., Gruber, N., Key, R. M., Lee, K., Bullister, J. L., Wanninkhof, R., Wong, C. S., Wallace, D. W. R., Tilbrook, B., Millero, F. J., Peng, T.-H., Kozyr, A., Ono, T., and Rios, A. F.: The Oceanic Sink for Anthropogenic CO_2, Science, 305, 367–371, 2004.

Salisbury, J., Vandemark, D., Mahadevan, A., Jonsson, B., Hunt, C., Campbell, J., and McGillis, W.: Episodic riverine influence on surface DIC in the coastal Gulf of Maine, Estuarine, Coast. Shelf Sci., 82, 108–118, doi:10.1016/j.ecss.2008.12.021, 2009.

Salisbury, J. E., Vandemark, D., Hunt, C. W., Campbell, J. W., McGillis, W. R., and McDowell, W. H.: Seasonal observations of surface waters in two Gulf of Maine estuary-plume systems: relationships between watershed attributes, optical measurements and surface pCO_2, Estuarine, Coast. Shelf Sci., 77, 245–252, 2008.

Schuster, U. and Watson, A. J.: A variable and decreasing sink for atmospheric CO_2 in the North Atlantic, J. Geophys. Res., 112, C11006, doi:10.1029/2006JC003941, 2007.

Schuster, U., Watson, A. J., Bates, N. R., Corbière, A., Gonzalez-Davila, M., MEtzl, N., Pierrot, D., and Santana-Casiano, M.: Trends in North Atlantic sea-surface fCO_2 from 1990 to 2006, Deep-Sea Res. Pt. II, 56, 620–629, 2009.

Shadwick, E. H., Thomas, H., Azetsu-Scott, K., Greenan, B. J. W., Head, E., and Horne, E.: Seasonal variability of dissolved inorganic carbon and surface water pCO2 in the Scotian Shelf region of the Northwestern Atlantic, Mar. Chem., doi:10.1016/j.marchem.2010.11.004, 2011a.

Shadwick, E. H., Thomas, H., Chierici, M., Else, B., Fransson, A., Michel, C., Mucci, L. A. M. A., Niemi, A., Papakyriakou, T. N., and Tremblay, J. E.: Seasonal variability of the inorganic carbon system in the Amundsen Gulf region of the southeastern Beaufort Sea, Limnol. Oceanogr., 2011b.

Shumway, R. H. and Stoffer, D. S.: Time Series Analysis and Its Applications With R Examples, Second Edition, Springer, New York, NY, USA, 2006

Strickland, J. D. H. and Parsons, T. R.: A practical handbook of seawater analysis, B. Fish. Res. Board Can., 167, 1–310, 1972.

Sweeney, C., nd Andrew R. Jacobson, E. G., Key, R. M., McKinley, G., Sarmiento, J. L., and Wanninkhof, R.: Constraining global air-sea gas exchange for CO_2 with recent bomb ^{14}C measurements, Global Biogeochem. Cycles, 21, GB2015, doi: 10.1029/2006GB002784, 2007.

Takahashi, T., Sutherland, S. C., Sweeney, C., Poisson, A., Metzl, N., Tilbrook, B., Bates, N. R., Wanninkhof, R., Feely, R. A., Sabine, C. L., Olafsson, J., and Nojiri, Y.: Global sea-air CO_2 flux based on climatological surface ocean pCO_2, and seasonal biological and temperature effects, Deep-Sea Res. Pt. II, 49, 1601–1622, 2002.

Takahashi, T., Sutherland, S. C., Wanninkhof, R., Sweeney, C., Feely, R. A., Chipman, D. W., Hales, B., Friederich, G., Chavez, F., Sabine, C., Watson, A., Bakker, D. C., Schuster, U., Metzl, N., Yoshikawa-Inoue, H., Ishii, M., Midorikawa, T., Nojiri, Y., Krtzinger, A., Steinhoff, T., Hoppema, M., Olafsson, J., Arnarson, T. S., Tilbrook, B., Johannessen, T., Olsen, A., Bellerby, R., Wong, C., Delille, B., Bates, N., and de Baar, H. J.: Climatological mean and decadal changes in surface ocean pCO_2, and net sea-air CO_2 flux over the global oceans, Deep-Sea Res. Pt. II, 56, 554–577, 2009.

Taylor, A. H., Geider, R. J., and Gilber, F. J. H.: Seasonal and latitudinal dependencies of phytoplankton carbon-to-chlorophyll a ratios: Results of a modelling study, Mar. Ecol. Prog. Ser., 152, 51–66, 1997.

Thomas, H., Bozec, Y., Elkalay, K., and de Baar, H. J. W.: Enhanced Open Ocean Storage of CO_2 from Shelf Sea Pumping, Science, 304, 1005–1008, 2004.

Thomas, H., Bozec, Y., Elkalay, K., de Baar, H. J. W., Borges, A. V., and Schiettecatte, L.-S.: Controls of the surface water partial pressure of CO_2 in the North Sea, Biogeosciences, 2, 323–334, doi:10.5194/bg-2-323-2005, 2005.

Thomas, H., Prowe, A. E. F., van Heuven, S., Bozec, Y., de Baar, H. J. W., Schiettecatte, L.-S., Suykens, K., Koné, M., Borges, A. V., Lima, I. D., and Doney, S. C.: Rapid decline of the CO_2 buffering capacity in the North Sea and implications for the North Atlantic Ocean, Global Biogeochem. Cycles, 21, GB4001, doi: 10.1029/2006GB002825, 2007.

Thomas, H., Prowe, F., Lima, I. D., Doney, S. C., Wanninkhof, R., Greatbatch, R. J., Schuster, U., and Corbière, A.: Changes in the North Atlantic Oscillation influence CO_2 uptake in the North Atlantic over the past 2 decades, Global Biogeochem. Cycles, 22, GB4027, doi:10.1029/2007GB003167, 2008.

Thompson, D. W. and Wallace, J. M.: Regional Climate Impacts of the Northern Hemisphere Annular Mode, Science, 293, 85–89, 2001.

Tsunogai, S., Watanabe, S., Nakamura, S., Ono, T., and Sato, T.: A preliminary study of carbon system in teh East China Sea, J. Oceangr., 53, 9–17, 1997.

Tsunogai, S., Watanabe, S., and Sato, T.: Is there a "continental shelf pump" for the absorption of atmospheric CO_2?, Tellus, 51, 701–712, 1999.

Ullman, D. J., McKinley, G. A., Bennington, V., and Dutkiewicz, S.: Trends in the North Atlantic carbon sink: 1992-2006, Global Biogeochem. Cycles, 23, GB4011, doi:10.1029/2008GB003383, 2009.

Umoh, J. U. and Thompson, K. R.: Surface heat flux, horizontal advection, and the seasonal evolution of water temperature on the Scotian Shelf, J. Geophys. Res., 99, 20403–20416, 1994.

Vandemark, D., Salisbury, J. E., Hunt, C. W., Shellito, S., and Irish, J.: Temporal and spatial dynamics of CO_2 air-sea flux in the Gulf of Maine, J. Geophys. Res., doi:10.1029/2010JC006408, 2010.

Wang, S. L., Chen, C. T. A., Hong, G. H., and Chung, C. S.: Carbon dioxide and related parameters in the East China Sea, Cont. Shelf Res., 20, 525–544, 2000.

Wanninkhof, R.: Relationships between wind speed and gas exhange over the ocean, J. Geophys. Res., 97, 7373–7382, 1992.

Wanninkhof, R., Olsen, A., and Trinanes, J.: Air-sea CO_2 fluxes in the Caribbean Sea from 2002-2004, J. Mar. Sys., 66, 272–284, 2007.

Watson, A. J., Schuster, U., Bakker, D. C. E., Bates, N. R., Corbiére, A., González-Dávila, M., Friedrich, T., Hauck, J., Heinze, C., Johannessen, T., Körtzinger, A., Metzl, N., Olafsson, J., Olsen, A., Oschlies, A., Padin, X. A., Pfeil, B., Santana-Casiano, J. M., Steinhoff, T., Telszewski, M., Rios, A. F., Wallace, D. W. R., and Wanninkhof, R.: Tracking the Variable North Atlantic Sink for Atmospheric CO_2, Science, 326, 1391–1393, 2009.

Weeks, A., Conte, M. H., Harris, R. P., Bedo, A., Bellan, I., Burkill, P. H., Edwards, E. S., Harbour, D. S., Kennedy, H., and Llewellyn, C.: The physical and chemical environment and changes in community structure associated with bloom evolution: the JGOFS North Atlantic Bloom Experiment, Deep-Sea Res. Pt. II, 40, 347–368, 1993.

Weiss, R. F.: Carbon dioxide in water and seawater: The solubility of a non-ideal gas, Mar. Chem., 2, 203–215, 1974.